AIAA JOURNAL
Vol. 41, No. 8, August 2003

Sectional Flow Structures in Near Wake of Elevated Jets in a Crossflow

Rong F. Huang* and Ren H. Hsieh†
National Taiwan University of Science and Technology, Taipei 10672, Taiwan, Republic of China

Near-wake flow structures in the symmetry and horizontal planes of elevated jets in a crossflow are studied experimentally in a wind tunnel via a laser Doppler velocimeter. The measured velocity vector fields and the corresponding streamline patterns in the symmetry and several horizontal planes display tremendous variations in different characteristic regimes of jet-to-crossflow momentum flux ratios. They are typically termed crossflow-dominated, transitional, and jet-dominated regimes. The complex flow behaviors are the result of the interactions among the downwash effect, which is induced by the crossflow passing over the tube tip; the upshear effect induced by the issuing jet; and the wakes behind the jet and the tube. Topological flow patterns are proposed to delineate the measured flow structures. Impact effects of the crossflow on the jet are discussed in two aspects, that is, the geometry and the turbulence properties of the central streamline. The geometric characteristics of the deflected jet in different flow regimes are presented and compared with previous results. The velocity components and turbulence properties along the central streamlines of different flow patterns show that the premier turbulence generation that is observed in this flow arrangement occurs in the impingement and jet bend over regions.

Nomenclature

D	=	outer diameter of tube, 6.4 mm
d	=	inner diameter of tube, 5 mm
H_j	=	maximum height of a central streamline, measured from level of tube tip to highest level of central streamline
R	=	jet-to-wind momentum flux ratio, $\rho_j u_j^2/\rho_w u_w^2$
Re_j	=	exit Reynolds number of jet, $u_j d/\nu$
Re_w	=	freestream Reynolds number of crossflow, $u_w D/\nu$
u, v, w	=	local velocity components in x, y, and z directions
u_j	=	average exit velocity of jet
u_w	=	freestream velocity of crossflow
u', v', w'	=	instantaneous velocity fluctuations in x, y, and z directions
$\overline{u'w'}$	=	Reynolds shear stress
x, y, z	=	Cartesian coordinates with origin at center of jet exit plane
x_0	=	originated locations on tube-opening plane from where bifurcation line evolves
θ_j	=	deflection angle of jet streamline evolving from origin on tube-opening plane
ν	=	kinematic viscosity of air
ρ_j	=	mass density of jet fluid
ρ_w	=	mass density of crossflow

Introduction

THE subject of the jet in a crossflow has been widely studied due to its wide range of industrial applications. It is commonly identified in two categories, according to the difference between the emerging sources of the jet. The jet may eject from an opening on a wall or from an elevated stack. A jet issuing from a wall opening into a crossflow is often encountered in the film cooling of jet engines, power plant combustors, vertical/standard takeoff and landing V/STOL, turbine-blade cooling, etc. An elevated jet discharging into a crossflow arises in many situations of technological importance of environmental field, for example, stack flare and plume dispersion. The wall-issued case is characterized by three-dimensional flows, which are subject to the interactions among the jet, jet wake, and wall boundary layer. The flow structures in the stack-issued case are subject to the interactions among the jet, jet wake, and stack wake. Flow properties of the jets emitted into crossflows from both ground-level sources and elevated sources have been examined in detail in the literature, but with more attention focused on the ground-level case.

Most of the studies on the wall-issued jet in crossflow before the mid-1980s dealt with the shape and centerline trajectory of the jets. The kidney-shaped counter-rotating vortices in the far field of the bent jets were also studied.[1–9] Mean and fluctuating velocity properties at jet-to-crossflow velocity ratios 0.5, 1, and 2 were studied by Andreopoulos and Rodi[10] and Andreopoulos.[11] They used a three-component hot-wire anemometer and reported the flow and turbulence properties in the jet wake and the wall boundary layer. Reverse flow was found to be restricted to a region very close to the wall. Sherif and Pletcher[12] conducted measurements of the velocity and turbulence characteristics of the jet in crossflow at jet-to-crossflow velocity ratios 4 and 6 in a water tunnel with hot-film probes. Two mean velocity maxima on the distribution profile of each vertical cross section in the symmetry plane were found. One is in the jet wake, which is usually a local maximum. The other is on the jet centerline trajectory, which is an absolute maximum. The double-peak behavior in the mean velocity profiles has also been observed by Andreopoulos and Rodi.[10] The turbulence intensity has an absolute maximum at the location of maximum velocity gradient and a local maximum near the wall surface in the wake region. Blanchard et al.[13] analyzed the wall-issued jet in crossflow and concluded that the longitudinal structures must be taken into account in the mechanism of stability. Examinations of the time-dependent coherent structures have been limited to spectral measurements[14–16] and flow visualizations.[17,18]

For the case of stack-issued jet in crossflow, few investigation results have been reported. Moussa et al.[19] have made similarity considerations on the Navier–Stokes equations for two geometrically, kinematically, and dynamically similar flows. They concluded that the bending geometry of two jets must be the same and can be related directly to the jet-to-crossflow momentum flux ratio. Also, the dimensionless ratios that govern the similarity in the nonbuoyant flowfield of jet-in-crossflow are the Reynolds numbers of the jet and crossflow, jet-to-crossflow momentum flux ratio, Strouhal

Received 22 March 2001; revision received 6 June 2002; accepted for publication 25 January 2003.

*Professor, Department of Mechanical Engineering. Senior Member AIAA.
†Graduate Student, Department of Mechanical Engineering.

number, and the shape factor. Andreopoulos[20,21] presented hot-wire anemometer-measured velocity profiles and statistical turbulence properties in the bent jet and the far-wake region of a cooling tower at low jet-to-wind velocity ratios. The results disclosed the strong interaction among the bent plume, cooling tower, and the wakelike region behind the cooling tower and jet. However, the detailed flow structures in the near-wake region behind the cooling tower and the deflected jet were not reported because of the limitations of instrumentation. More recently, Eiff et al.[22] and Eiff and Keffer[23] used the pattern-recognition technique to study the coherent structures within the near-wake region of a turbulent tube-discharged jet in a crossflow. They found that the von Kármán-like vortex structures in the wake of the pipe are locked to similar structures in the jet wake.

Because the large structures in the near wake of the tube-issued jet in crossflow are still unclear, the aim of this paper is to reveal the characteristics of the flows in this area. The streamline patterns, velocity distributions, and turbulence properties along the central streamline are investigated.

Experimental Setup

Crossflow and Jet

The crossflow was supplied by an open-circuit wind tunnel, as shown in Fig. 1. The wind tunnel had a test section $30 \times 30 \times 110$ cm in size. The floor of the test section was made of an aluminum-alloy plate. The lateral walls and the ceiling were made of glass plates for transmission and receiving of laser lights. At $Re_w = 2074$, a parallel flow velocity profile with a nonuniformility of about 0.8% was detected at the stage $x/d = -20$ by using a two-component laser Doppler velocimeter. The turbulence intensity was less than 0.25%. The average wind velocity was detected with a retractable pitot static tube and a high-precision electronic pressure transducer. The pitot static tube was retracted to the floor of the test section when the velocity measurements were conducted to not influence the flow field.

The elevated stack was a stainless steel tube with an inner diameter 5.0 mm, outer diameter 6.4 mm, and length 560 mm. The tube protruded perpendicularly 160 mm into the aluminum floor plate of the test section. Positions are described in terms of a rectangular coordinate system (x, y, z), as shown in the subset of Fig. 1. The origin of the coordinate system was centered at the exit plane of the tube. The stack tube was adapted to the tip of a nozzle assembly. The nozzle assembly served as a flow-conditioning device in which honeycombs and three layers of mesh screens were installed. The jet flow rate was measured by a set of rotameters and was constantly checked with a laminar flow meter. The average exit velocity profiles measured by a two-component laser Doppler velocimeter were parabolic for Reynolds number Re_j less than about 3000. At larger Reynolds numbers, transition of flow occurs. The turbulence intensity of the jet at $(x/d, y/d, z/d) = (0, 0, 0.04)$ was lower than 0.35% for Re_j less than about 3000. At larger Reynolds numbers, the turbulence intensity at the jet exit increases to about 2.5%.

During the experiment, the crossflow Reynolds number Re_w was set at 2074. The jet Reynolds number Re_j based on the inner diameter of the tube was varied from 200 to 8000. The jet-to-crossflow momentum flux ratio thus covered a wide range from 0.015 to 25.

Velocity Measurements

The velocity field was measured with a two-component laser Doppler velocimeter (LDV). The blue and green laser beams, which were supplied by a Spectra-Physics Stabilite-2017 6-W argon-ion laser, were separated and focused through the Dantec Fiber-Flow optical system. The dimensions of the measuring volumes of the green and blue components estimated at e^{-2} light intensity level were about $0.120 \times 0.120 \times 1.543$ mm and $0.114 \times 0.114 \times 1.463$ mm, respectively. The fringe separations of these components were 3.31 and 3.14 μm, respectively. The system was configured to operate at backscatter mode. A Bragg cell was embedded in the system to distinguish the directional ambiguity. A Dantec flow velocity analyzer enhanced two-component correlation processor was used to convert the Doppler signals into frequency data. The frequency data were fed into a personal computer-controlled data acquisition system to calculate the velocities and other statistical properties. Each velocity data record consisted of 6000 samples, which would last for about 0.8 s. The average sampling rate was about 7.5 kHz. When 0.21 was taken for the Strouhal number of the tube-wake vortex shedding at $Re_w = 2074$, the shedding frequency was about 150 Hz.

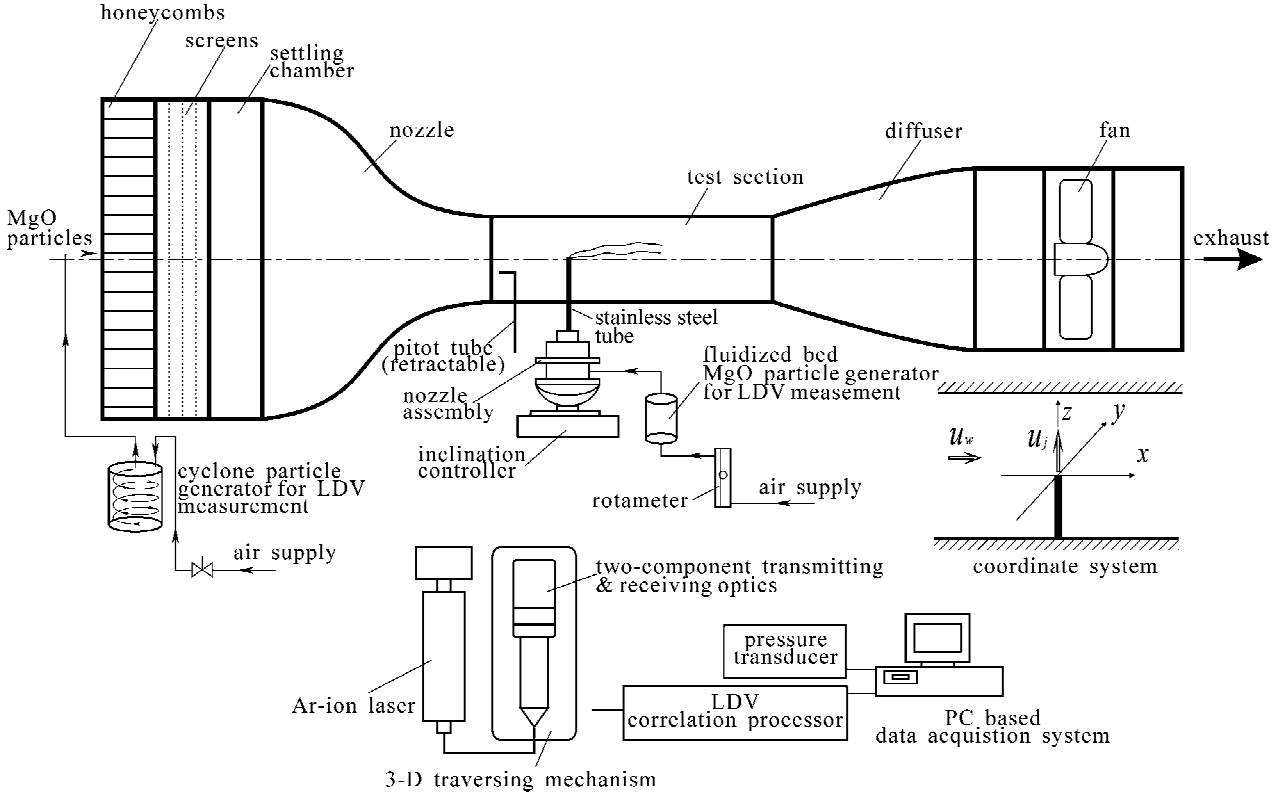

Fig. 1 Experimental setup.

Approximately 120 cycles of the wake dynamic structures was contained in a data record for calculations of average and turbulence properties. When the frequency of the coherent structures on the jet was considered, 400 ~ 1000 Hz was detected by using a hot-wire anemometer. Hence, at least 300 cycles would be captured in a data record for data processing. Two sets of three-component traversing mechanisms with a resolution of 10 μm were set up on one side and on the top of the test section, respectively. Depending on the measurements being conducted for the symmetric or horizontal planes, the transmitting/receiving optics of the LDV was installed and precisely mounted on the side or the top traversing mechanism.

Magnesium oxide particles with an average diameter of 5 μm were introduced into both the jet and the crossflow to scatter the laser light via two separated particle seeders. A cyclone particle generator as described by Glass and Kennedy[24] was used for the crossflow seeding, and a fluidized bed was installed for the jet seeding. The particles were estimated to be capable of following frequencies up to 3.6 kHz (Ref. 25).

Uncertainties

The accuracy of the measurement of freestream velocity was affected primarily by the alignment of pitot tube and the calibration of the pressure transducer. With the help of an online micropressure calibration system and the careful alignment of the pitot tube, the uncertainty in the freestream velocity was estimated[26] to be as large as 3% of reading. The rotameters used to measure the flow rate of the air jet were calibrated in the laboratory with a microflow calibration system. The accuracy was ±1% of full scale. The estimated uncertainties of the LDV measurements were less than 1% for the mean velocities and 7% for the turbulence intensities and Reynolds stresses.

Results and Discussion

Tomographic Flow Structures

Crossflow-Dominated Regime

Figure 2 shows the velocity vectors and the streamline patterns in the symmetry plane of the near wakes at various jet-to-crossflow momentum flux ratios. The spacing between the measurement points is $0.084d$ in the region close to the tube tip. In other regions, it varies from $0.1d$ to $0.6d$. The measurement points are dense in the near-wake region and sparse in the far field. When shown, superfluous velocity vectors are removed for clarity of presentation. The streamlines are obtained by using the shooting method.

At $R = 0.1$, as shown in Fig. 2a, the jet momentum is not large enough to sustain the impingement of the transverse stream so that the streamlines evolving from the tube opening are deflected through large angles from the vertical axis of the tube. A downwash area is enclosed between a dividing streamline evolving from $(x/d, z/d) = (0.04, 0)$ and the tube. This dividing streamline is a bifurcation line in topological terms.[27,28] At the jet exit, the streamlines emanating from the left of the bifurcation line extend downstream, whereas those emitting from the right of the bifurcation line go into the downwash area. With the increase of the jet momentum, a vortex is formed in the jet wake due to the interaction between the jet shear and the downwash effect, as shown in Fig. 2b. A bifurcation line, which separates the downwash and downstream areas, evolves from $(x/d, z/d) = (0.32, 0)$. Figure 3 shows the originated

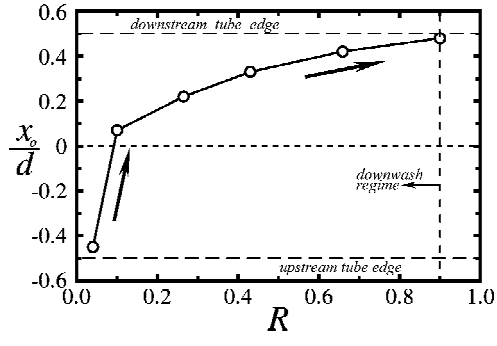

Fig. 3 Locations on the tube opening from where the bifurcation lines originate, $Re_w = 2074$.

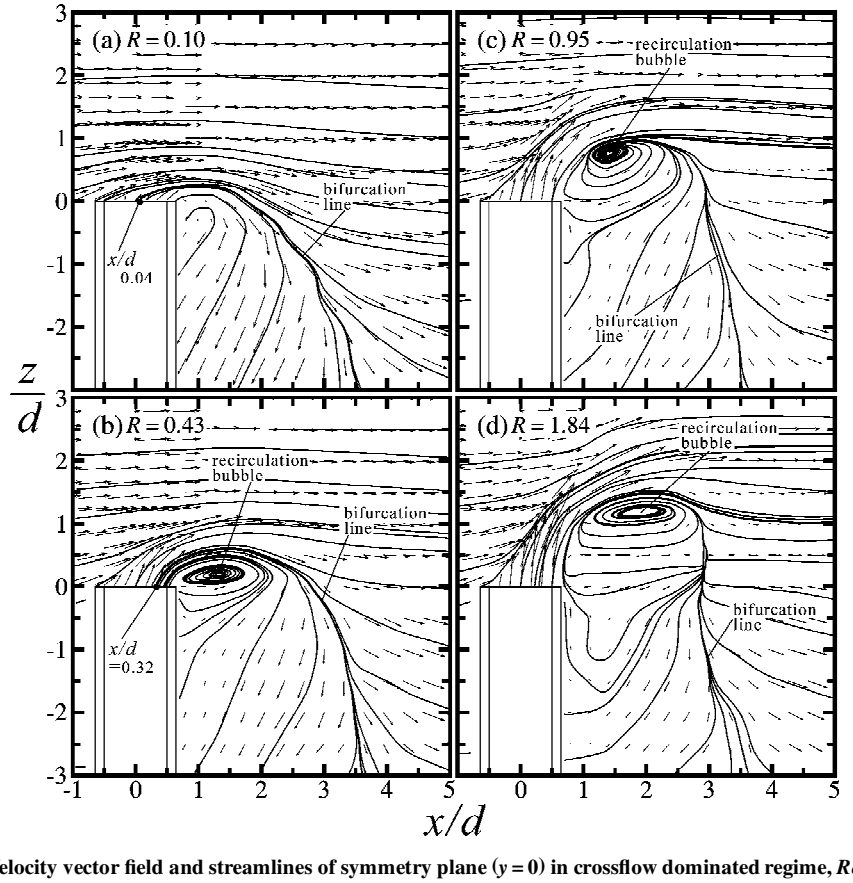

Fig. 2 Velocity vector field and streamlines of symmetry plane ($y = 0$) in crossflow dominated regime, $Re_w = 2074$.

locations of the bifurcation lines at various R. For $R < 0.9 \pm 0.03$, all of the bifurcation lines evolve from the tube opening, that is, $-0.5 < x_0/d < 0.5$. When R is greater than about 0.9, all streamlines emitting from the tube opening go directly to the downstream area. At $R < 0.9 \pm 0.03$, part of the jet-issued fluids in the symmetry plane would be downwashed into the recirculation region in the near wake behind the tube, if diffusion and dispersion are not considered. The uncertainties for the range of the characteristic flow regimes were estimated according to the flow patterns of LDV measurements at many R. The differences between neighboring regimes were pretty distinct, so that the identification was not very difficult. To achieve this, flow patterns were measured at many R around the critical values.

At larger values of R, as shown in Figs. 2c and 2d, the jets shoot up a little higher than at the values shown in Figs. 2a and 2b before they are deflected into the crossflow direction. Compared with that in Fig. 2b, the jet-wake vortex becomes larger and is located at a higher level. It is even more apparent in Fig. 2d. The bifurcation lines shown in Figs. 2c and 2d do not evolve from the tube opening. Instead, they evolve from the jet-wake vortices. All of the streamline patterns of the flows at $R < 1.9 \pm 0.03$ show features similar to those shown in Figs. 2c and 2d. A term crossflow-dominated regime is applied.

The flow patterns of the horizontal planes at $R = 0.95$ are shown in Fig. 4. In Fig. 4a for $z/d = 0.6$, the crossflows wrap across the jet and turn around to form a recirculation bubble. Two stagnation points exist on the symmetry axis. A forward stagnation point is located at $x/d = 0.56$. An aft stagnation point is located at $x/d = 2.67$. The axial bubble length is about $2.11d$. The streamline evolves laterally from the forward stagnation point and goes downstream. The bubble centers at a focus that is unstable[27,28] because the streamlines evolve from the focal center. The recirculation bubble in the horizontal plane is subject to the shear effect, which is developed by the up-shooting jet. The jet shoots up and deflects to the downstream area. The combined effects of the jet shear and the jet wake cause the recirculation bubble to form on the x–z plane, as shown in Fig. 2. It is expected from Figs. 2c and 4a that a three-dimensional recirculation bubble exists in the jet wake. In the plane $z/d = 0.1$, as shown in Fig. 4b, the focus becomes stable[27,28] because the streamline evolving laterally from the forward stagnation point goes into the focus. On the plane across the tube wake at $z/d = -2.0$, as shown in Fig. 4c, the forward stagnation point attaches to the tube wall, whereas the aft stagnation point is located far downstream at $x/d = 3.39$. The axial bubble length becomes $2.76d$, which is about 30% longer than that in the jet wake. The focus is unstable, as is that shown in the jet wake of Fig. 4a. The axial locations of the bifurcation line in the symmetry plane of Fig. 2c coincide with those of the aft stagnation points in the horizontal planes of Fig. 4. It is clear that the bifurcation line in the symmetry plane describes the loci of the aft stagnation points of the recirculation bubble of the jet and tube wakes.

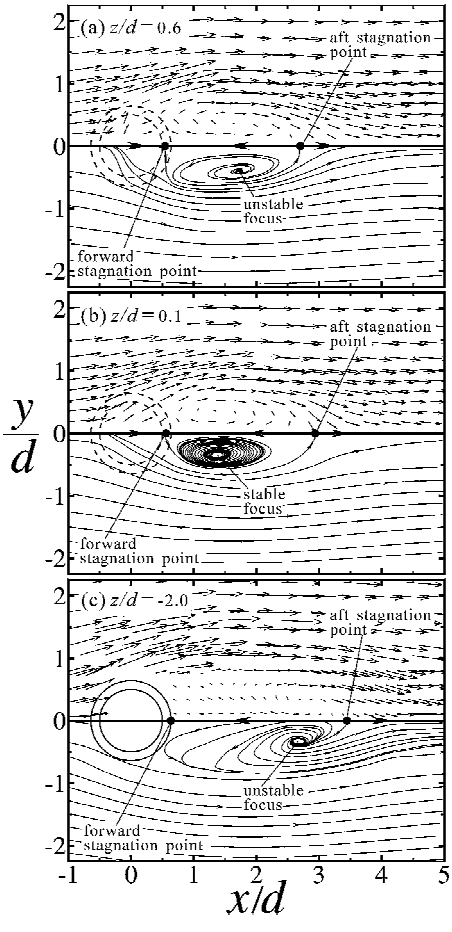

Fig. 4 Velocity vector field and streamlines of horizontal planes in crossflow-dominated regime, $R = 0.95$ and $Re_w = 2074$.

Transitional Regime

In the regime $1.90 \pm 0.03 < R < 5.90 \pm 0.10$, complex behaviors of flow transition proceed due to the competition between the up-shear effect of the jet and the downwash effect that is induced when the crossflow goes across the tube tip. Figures 5a–5d show three types of velocity vector field and streamlines at various R. Figure 5a shows type 1 of the transitional flow at $R = 2.02$. The momentum of the up-shooting jet is strong enough so that the jet-wake vortex in the crossflow-dominated regime shown in Fig. 2 is stretched off. Two flow structure features, that is, the reverse flows in the jet wake and the recirculation bubble in the tube-wake, are found. The reversed streamlines in the jet wake appear in the region near the jet because of the up-shear effect of the up-shooting jet. Consequently, because of the shear of the bent jet the streamlines point rightward and eventually extend to the downstream area. Near the leeside of the tube tip, a clockwise-rotating recirculation region centered around $(x/d, z/d) = (1.4, -0.8)$ is induced because of the combined effects of the up-shear jet and the downwash flow. A bifurcation line standing at $x/d \approx 3.4$ below the jet exit plane describes the loci of the aft stagnation points of the recirculation bubbles on the horizontal planes in the tube wake.

Figure 5b shows the velocity vectors and the streamlines of type 2 transitional flow at $R = 2.40$. Because of the increase of jet momentum, a counterclockwise-rotating vortex located behind the up-shooting jet and above the lee side of tube tip is formed. The vortex is formed due to the interactions among the up-shear jet, jet-wake reverse flow, and the tube-wake recirculation bubble. A jet-wake vortex similar to the one observed here has also been found by Brizzi et al.[18] in an experiment for a wall-issued water jet that was submerged into a crossflow at $Re_w = 251$ and $R = 6.25$. Two saddle points are consequently formed to satisfy the flow topology. One of them is between the up-shear jet and the counterclockwise-rotating jet-wake vortex. The other one is located between the clockwise-rotating tube-wake vortex and the reverse flow region in the jet wake. A source point comes up between the bifurcation lines of the jet-wake and the tube-wake.

Figures 5c and 5d show the velocities and the streamlines of type 3 transitional flow at $R = 2.70$ and 4.43, respectively. Huge up-shear effect developed by the jet suppresses the downwash effect so that the streamlines, which evolve from the tube-wake bifurcation line toward the leeside of the tube, become flatter. Consequently, the tube-wake recirculation vortex and its accompanying saddle point shown in Fig. 5d disappear.

Figure 6 shows the sectional flow structures of various horizontal planes in the type 3 transitional regime at $R = 2.70$. The flow structures in the jet wake on the planes $z/d = 2.0$ and 1.0, as shown in Figs. 6a and 6b, respectively, are similar to that in Fig. 4a. The bubble structures located between the forward and aft stagnation points with unstable foci[27,28] are found. The flow structure in the tube wake on the plane $z/d = -2.0$, as shown in Fig. 6f, is similar to that in Fig. 4c. However, the sectional flow structures shown in Figs. 6c–6e display quite different patterns around the area of interface between the jet and the tube wakes. Because the horizontal plane $z/d = 0.5$

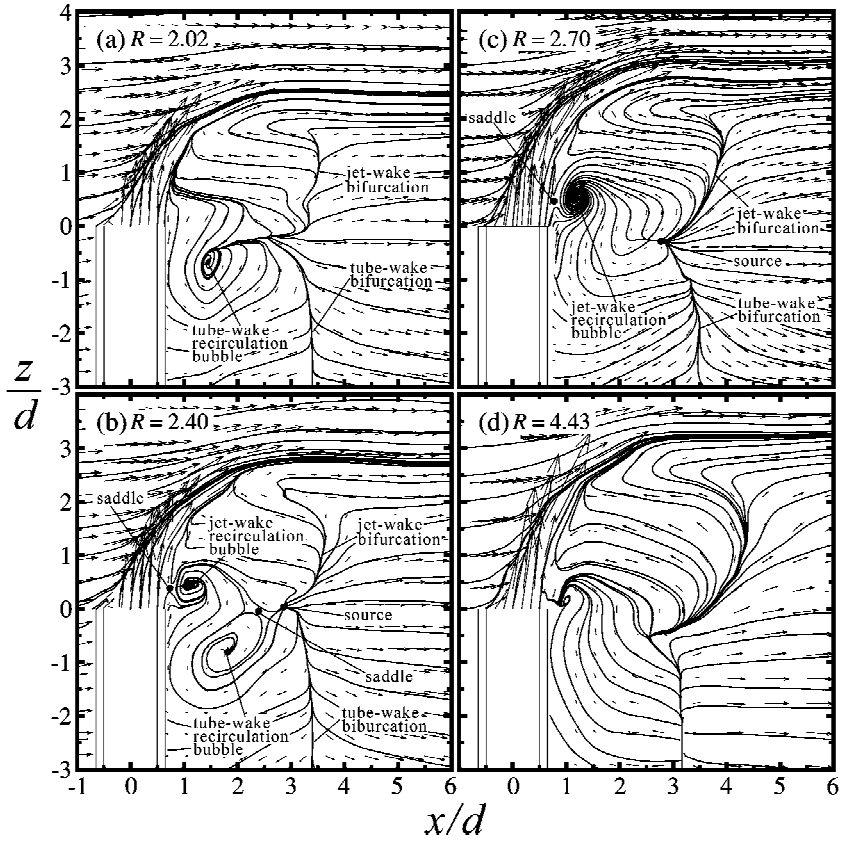

Fig. 5 Velocity vector field and streamlines of symmetry plane ($y = 0$) in transitional regime, $Re_w = 2074$: a) type 1, b) type 2, c) type 3, and d) type 3.

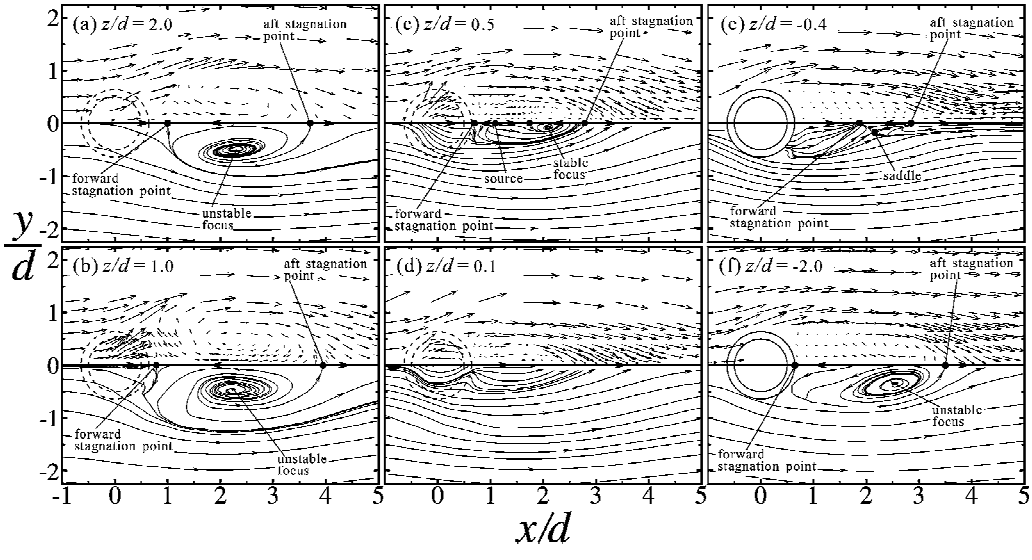

Fig. 6 Velocity vector field and streamlines of horizontal planes in transitional regime, $R = 2.70$ and $Re_w = 2074$.

of Fig. 6c goes across the saddle point and the jet-wake bubble of Fig. 5c, four stagnation points on the symmetry axis $y/d = 0$ and a bubble structure of stable focus[27,28] are formed. All four stagnation points can find their counterparts of null axial velocities in Fig. 5c. The forward stagnation point is located near the jet-wake saddle point of Fig. 5c. The aft stagnation point located at $x/d = 2.80$ corresponds to the point with a zero u velocity component on the level across $z/d = 0.5$ in Fig. 5c. Between the forward and aft stagnation points of Fig. 6c, there are two extra stagnation points. These two stagnation points describe the left and the right boundaries of the jet-wake vortex across the line $z/d = 0.5$ in Fig. 5c. On the plane $z/d = 0.1$, as shown in Fig. 6d, no stagnation point is found on the axis $y/d = 0$ because all of the u velocity components along the line $z/d = 0.1$ of Fig. 5c are positive. Below the tube-tip plane, as shown in Fig. 6e, an off-axis saddle and two stagnation points appear on the symmetry axis $y/d = 0$. The forward stagnation point is a sink, whereas the aft one is a source. It is evident that the detailed flow structures around the interface area between the jet and the tube wakes of the transitional flows are very complicated. Above and below the interface area, the sectional flow structures are similar to those observed in the crossflow-dominated regime.

Jet-Dominated Regime

In the regime $R > 5.90 \pm 0.10$, the jet momentum is large enough to sustain the impact of the transverse stream so that the velocity vectors emitting from the jet exit do not deflect appreciably from the

Table 1 Ranges of R values for different characteristic flow patterns at $Re_w = 2074$

Characteristic flow	Range of R
Crossflow dominated	$R < 1.9 \pm 0.03$ ($R < 0.9 \pm 0.03$ downwash)
Transitional	$1.9 \pm 0.03 < R < 5.9 \pm 0.10$
Jet dominated	$5.9 \pm 0.10 < R$

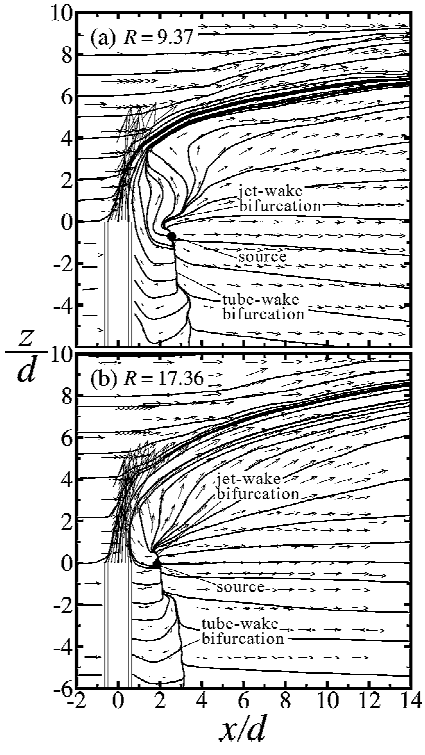

Fig. 7 Velocity vector field and streamlines of symmetry plane ($y = 0$) in jet-dominated regime, $Re_w = 2074$.

vertical direction, as exemplified in Fig. 7. In Fig. 7a, the deflection angle of the jet is small in the region $0 < z/d < 3$. In the region where z/d is higher than about 3, the up-shooting jet loses a large amount of momentum flux so that the velocity vectors are deflected appreciably to point to the right due to the impingement of the crossflow. At $z/d > 5$, the x components of the velocity vectors become much larger than the z components because the momentum exchanges significantly from the z direction to the x direction. In the jet wake, very strong up shear developed by the jet on the wake region causes the flow velocities near the leesides of the tube and the jet to point upward. The jet-wake saddle and the counterclockwise-rotating jet-wake vortex, which appear in Fig. 5 of the transitional flows, hence, are all stretched away. Only one source point located between the jet-wake and the tube-wake bifurcation lines is left in the flowfield. The jet-wake bifurcation line becomes short. In the tube wake, the bifurcation line goes downward and separates the flowfield into reverse and forward flow regions. The flows emitting from the source point must come from the lateral streams to satisfy the law of mass conservation. The lateral streams are induced by the recirculation bubble, as shown in Fig. 8 for $R = 17.36$. When Figs. 8a and 8c are compared, the bubble length of the jet wake is apparently much shorter than that of the tube wake. The recirculation bubble in the jet wake is an unstable focus,[27,28] whereas it is a stable focus in the tube wake. This situation also occurs in the crossflow-dominated and transitional regimes.

The ranges of R for different characteristic flow patterns at $Re_w = 2074$ are listed in Table 1. Although it is not shown here, it was observed in the laboratory that the critical values of R increase gradually with Reynolds number Re_w.

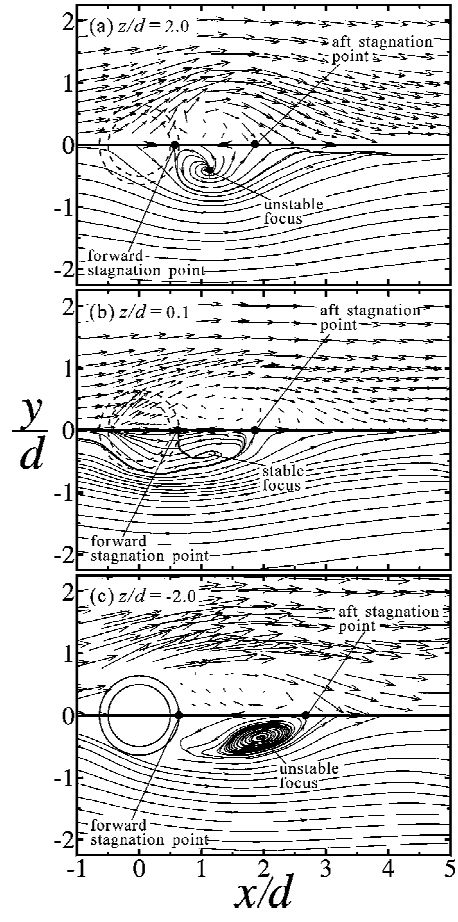

Fig. 8 Velocity vector field and streamlines of horizontal planes in jet-dominated regime, $R = 17.36$ and $Re_w = 2074$.

Maps of Topological Flow Patterns

Figure 9 shows the pictorial topological flow patterns of the near-wake flows in the symmetry plane. Following Perry and Fairlie[27] as well as Chong and Perry,[28] the topological flow pattern is characterized by critical points, separatrices, and alleyways. In topological terminology, a critical point is a point in a flowfield where the streamline slope is indeterminate, a separatrix is a streamline that leaves or terminates at a saddle, and an alleyway is a passageway in between the two separatrices. When the critical points, separatrices, and alleyways are correctly described, the flow map can be clearly delineated. In the present case, the critical points consist of saddles and nodes.

Figures 9a and 9b show the topological flow patterns in the crossflow-dominated regime. In Fig. 9a, the bifurcation line evolves from the tube opening, whereas in Fig. 9b the bifurcation line evolves from the jet-wake vortex. In both Figs. 9a and 9b, four three-way saddles, a leading-edge saddle S_1' on the tube tip, a stagnation point S_2' on the tube surface of the up-wind side, a trailing-edge saddle S_3' on the tube tip, and a reattaching point S_4' on the leeside of the tube surface, are formed. In addition, a node N_1 is also shown. Because the three-dimensional effect is almost unavoidable in real flows,[29] the focus instead of the center is presented. Hunt et al.[30] obtained a general formula for the relationship between the numbers of nodes (including four-way nodes N and three-way nodes N') and saddles (including four-way saddles S and three-way saddles S') for the flows around surface obstacles. The topological rule is

$$\left(\sum N + \frac{1}{2}\sum N'\right) - \left(\sum S + \frac{1}{2}\sum S'\right) = 1 - n$$

in which n is the connectivity of the section of the flow under consideration. In this case, $n = 2$ because one solid obstacle presents in the flowfield. When the number of the critical points is counted in

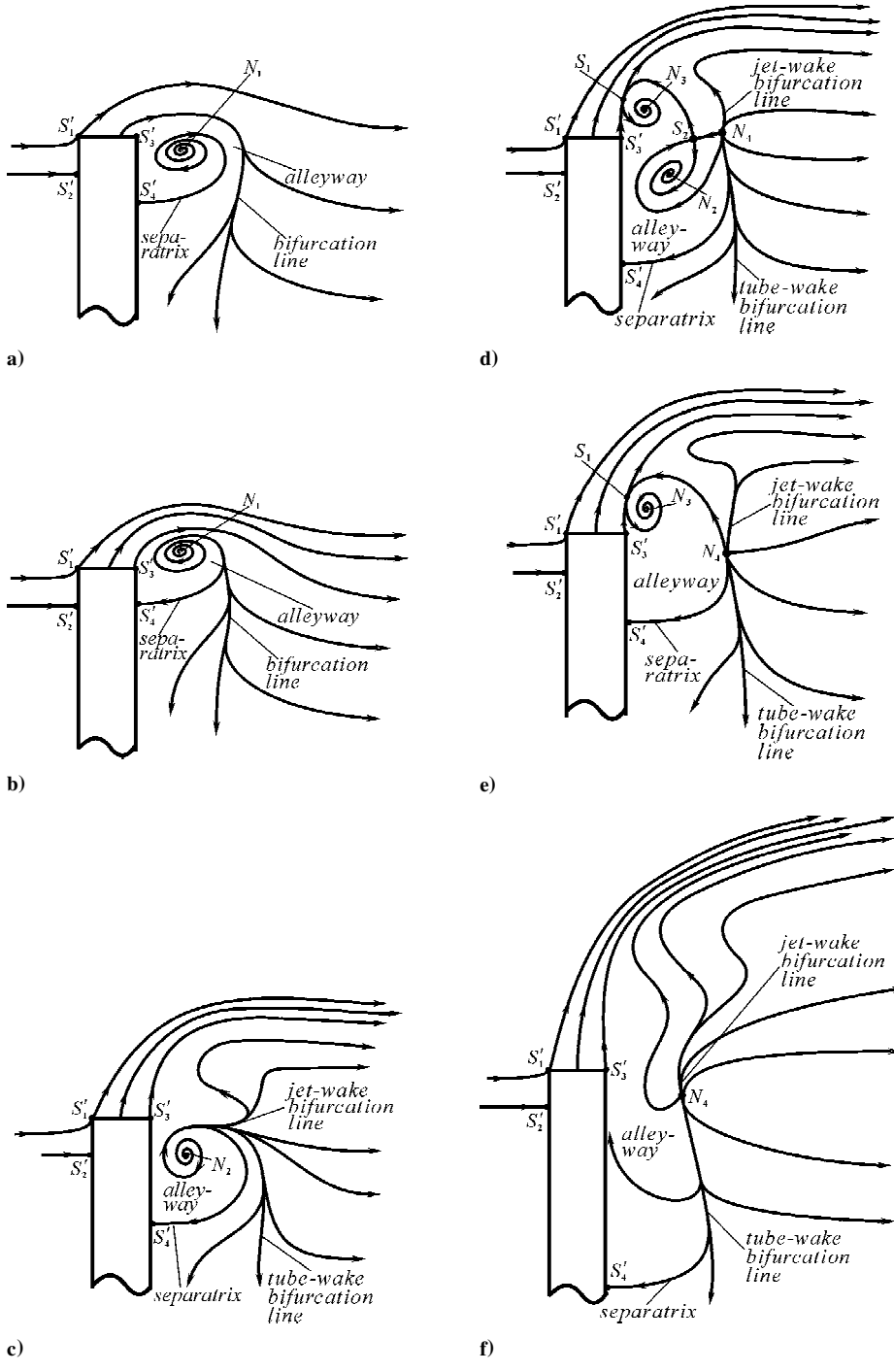

Fig. 9 Topological flow patterns of symmetry plane ($y = 0$): a) downwash flow, b) crossflow-dominated flow, c) type 1 transitional flow, d) type 2 transitional flow, e) type 3 transitional flow, and f) jet-dominated flow.

Fig. 9a or 9b, that is,

$$\sum N = 1, \qquad \sum N' = 0, \qquad \sum S = 0, \qquad \sum S' = 4$$

the topological rule is satisfied.

Figures 9c–9e show the flows in the transitional regime. As discussed earlier in the section of velocity vector field and streamlines, a tube-wake vortex, a pair of counter-rotating jet-wake and tube-wake vortices, and a jet-wake vortex feature the transitional flows of types 1, 2, and 3, respectively. These complex flow patterns are induced by the competition between the effects of the up shear and the downwash on the jet and tube wakes. Figure 9f shows the pictorial topological flow pattern in the jet-dominated regime. Only the source point N_4 exists in between the jet-wake and the tube-wake bifurcation lines.

The topological flow patterns of the horizontal planes are proposed in Fig. 10. In the jet wake, as shown in Fig. 10a, flows in all characteristic flow regimes have two fourway saddles (S_1 and S_2) and two nodes (N_1 and N_2). In this case, $n = 1$ because no solid obstacle presents in the sectional flowfield. When the number of critical points is counted, that is,

$$\sum N = 2, \qquad \sum N' = 0, \qquad \sum S = 2, \qquad \sum S' = 0$$

the topological rule

$$\left(\sum N + \frac{1}{2}\sum N'\right) - \left(\sum S + \frac{1}{2}\sum S'\right) = 1 - n$$

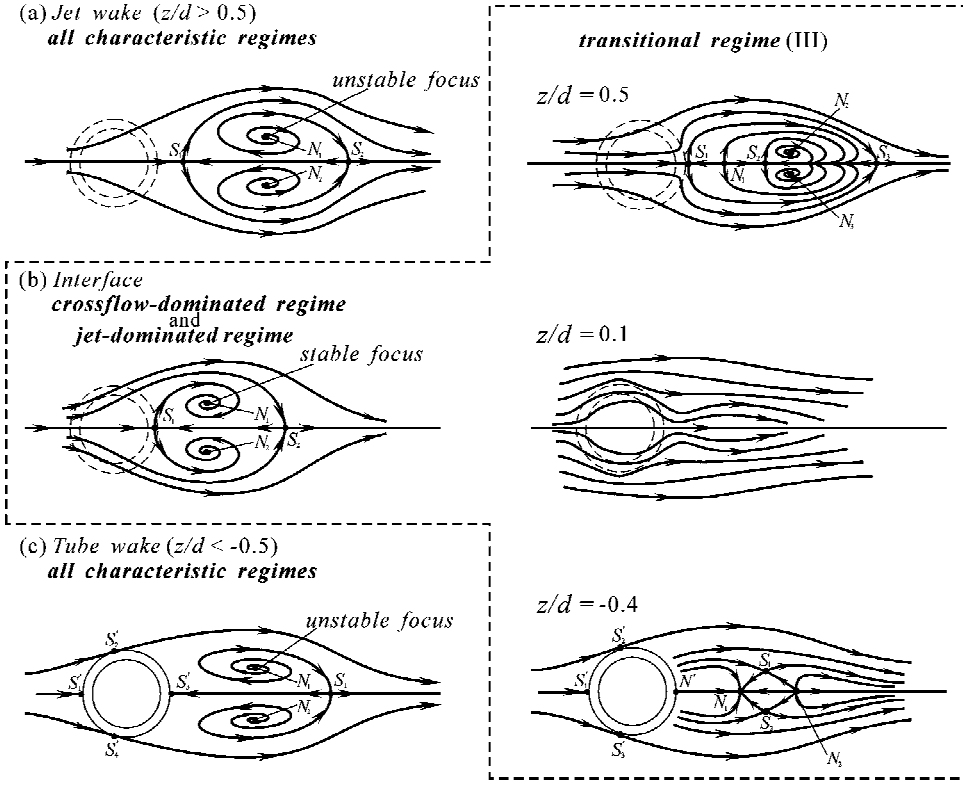

Fig. 10 Topological flow patterns of horizontal planes.

is satisfied. The forward stagnation point S_1 is a fourway saddle. The streamlines that evolve laterally from the forward stagnation point S_1 go downstream. The streamlines that go to the aft stagnation point S_2 are evolved from the unstable foci N_1 and N_2.

In the tube wake, as shown in Fig. 10c, flows in all characteristic regimes have four threeway saddles ($S_1' - S_4'$) on the tube wall: one four-way saddle S_1 on the symmetry axis, and two nodes N_1 and N_2. The forward stagnation point S_3' attaches to the leeside of the tube, so that it becomes a threeway saddle. S_1' is an upstream stagnation on the tube wall, whereas S_2' and S_4' are separation points of the boundary layers. The recirculation bubbles in the tube wake are centered at unstable foci N_1 and N_2, which is similar to those observed in the crossflow-dominated regime. In this case, $n = 2$ because one solid obstacle presents in the sectional flowfield. When the number of the critical points is counted, that is,

$$\sum N = 2, \qquad \sum N' = 0, \qquad \sum S = 1, \qquad \sum S' = 4$$

the topological rule

$$\left(\sum N + \frac{1}{2}\sum N'\right) - \left(\sum S + \frac{1}{2}\sum S'\right) = 1 - n$$

is satisfied.

Around the interface region, the situation is complex. For both the crossflow-dominated and jet-dominated regimes, as shown in Fig. 10b, two features different from Fig. 10a are observed. The separatrices, which evolve from the forward stagnation point S_1, do not go downstream as they do in the jet wake. Instead, they go into the vortex so that the vortex centers become stable foci. The streamlines that go into the aft stagnation point S_2 are evolved from upstream flows. For type 3 flow of the transitional regime, the topological flow patterns around the interface region are complex because of the existence of the jet-wake and tube-wake vortices, as shown in Fig 5.

Geometry Characteristics

The impact effect of the crossflow on the jet geometry can be observed from the maximum height and the deflection angle of the central streamline, shown in Fig. 11. Figure 11a shows the normalized maximum heights H_j/d of the central streamlines evolving from the center of the tube opening. In the crossflow-dominated and the transitional regimes, H_j/d increases fast with the increase of R. The increase rate becomes low in the jet-dominated regime. Some previous works[2,6,31,32] concerning the jet centerline trajectories are shown in Fig. 11a for comparison. At low R, the experimental result of Keffer and Baines[2] and the semi-analytical prediction of Sucec and Bowley[31] seem to be close to the present results. At large R, however, the deviation is notable. The experimental data employed by Keffer and Baines[2] to correlate the trajectory formula are

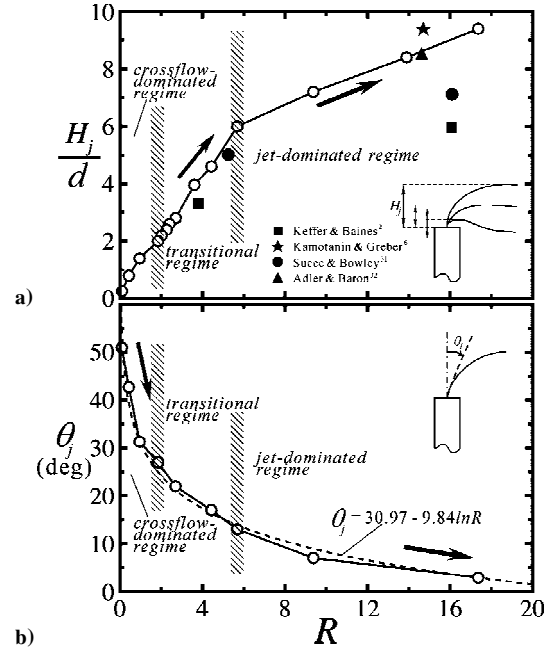

Fig. 11 Geometric properties of jet central streamline: a) maximum height of central streamline and b) deflection angle of central streamline at jet exit.

obtained from long-exposure smoke-trace flow-visualization pictures. They may subject to a great difficulty of identification at large R because of a severe turbulent diffusion problem. The result obtained by Adler and Baron[32] using a quasi-three-dimensional integral method shows a good agreement with the present measurement at large jet-to-crossflow momentum flux ratio 14.7. They do not recommend the application of that method to low R because of the inherent deficiency of the integral method. Kamotani and Greber's experiment,[6] in which a one-component hot-wire anemometer was applied, grows a little higher than the present result at large R.

The influence of the impact of the crossflow on the jet geometry can also be observed from the deflection angle of the central streamline at the jet exit, shown in Fig. 11b. The deflection angle decreases rapidly with the increase of R in the crossflow-dominated regime. When the jet momentum is large in the jet-dominated regime, the decreasing rate becomes relatively low. In this regime deflection angle is lower than about 13 deg. It is only 3 deg, which is negligibly small, at $R = 17.36$. The jet momentum in the jet-dominated regime is large enough to resist the impact of the crossflow so that the deflection angle is small and the maximum height of the central streamline is large.

Turbulence Properties Along Central Streamline

Figure 12 shows the central streamlines, normalized local velocities (u/u_w and w/u_w), and turbulence properties [$\sqrt{(u'^2)}/u_w$, $\sqrt{(w'^2)}/u_w$, and $\overline{u'w'}/u_w^2$] along the central streamline in three flow regimes. As shown in Fig. 12a, the central streamline for $R = 0.89$ in the crossflow-dominated regime shoots up a short distance to $z/d \approx 1.5$ and bends quickly to the right due to the impingement of the crossflow. Because of the low jet-to-crossflow momentum flux ratio, the downwash effect overwhelms the up-shooting momentum and "attracts" the central streamline to a level below the tube-tip plane. In the transitional regime at $R = 3.49$, the central streamline shoots up to a level $z/d \approx 3$, then turns to the right, and remains almost horizontal in the downstream area. In the jet-dominated regime, at $R = 13.83$, the central streamline is not deflected by a large angle until it shoots up to a high level, $z/d \approx 3.7$. The deflected central streamline still gradually goes up even at the downstream stage $x/d = 15$. It moves eventually in the freestream direction in the far downstream area for x/d greater than about $25d$.

The normalized local velocity distributions u/u_w, as shown in Fig. 12b, attain peak values where the central streamlines make turns. The peak value of u/u_w at $R = 13.83$ is smaller than that at $R = 3.49$ because the central streamline in the jet-dominated regime is less deflected around the jet-turning region than in other two regimes. The normalized local velocity distributions w/u_w, as shown in Figs. 12c, decrease rapidly from the jet exit, then approaches gradually to low constant values in the downstream area. For the crossflow-dominated flow, w/u_w remains at small negative values even at the downstream region $x/d = 25$. For the transitional flow, w/u_w approaches almost null when $x/d > 10$. For the jet-dominated flow, w/u_w remains positive and does not approach zero even at the downstream stage $x/d = 25$. From Figs. 12b and 12c, it appears that the change of jet momentum from the z component to the x component in the transitional regime is most efficient among three characteristic flow regimes.

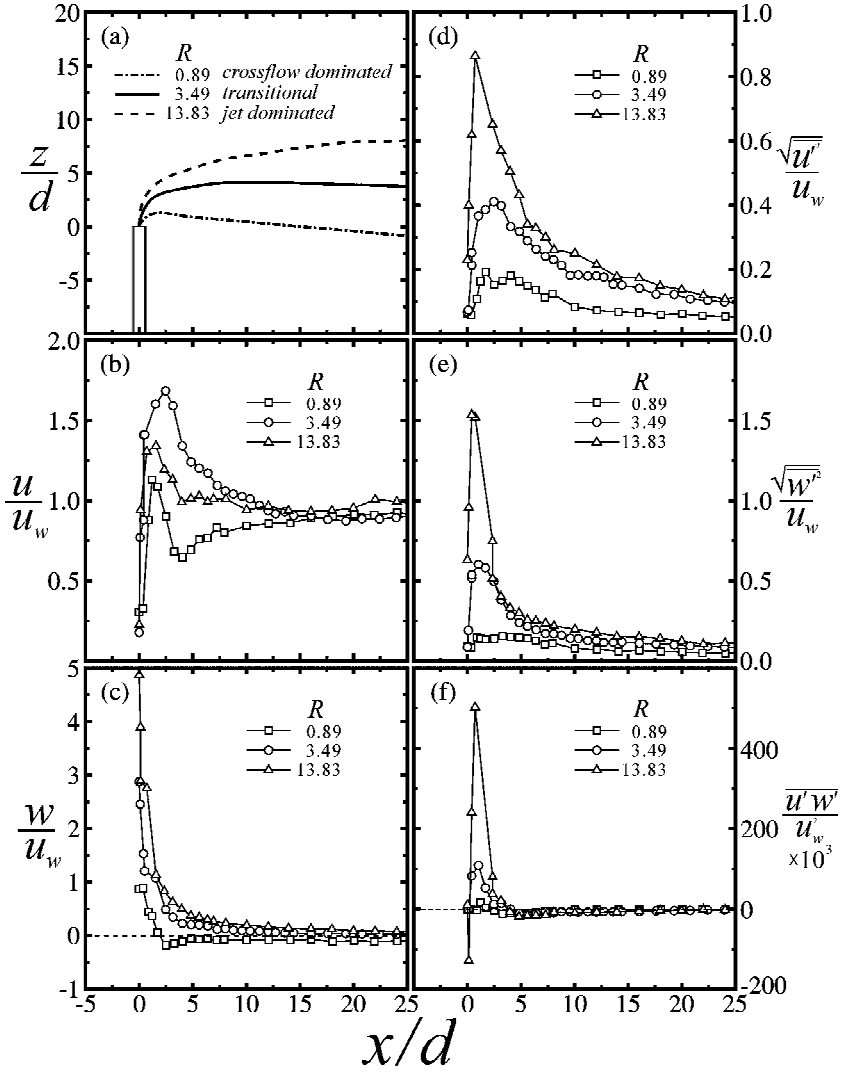

Fig. 12 Turbulence properties along central streamline.

The normalized turbulence properties $\sqrt{(\overline{u'^2})}/u_w$, $\sqrt{(\overline{w'^2})}/u_w$, and $\overline{u'w'}/u_w^2$ of the central streamlines are presented in Figs. 12d–12f. They increase quickly in a short axial distance before the central streamlines are bent due to the effects of impingement and shear developed by the crossflow. The peak values occur where the central streamlines make turns. The turbulence properties decrease drastically in a short distance after the jet bends, then approach constant values in the downstream region. Around the bend over region, the turbulences, which are induced by the momentum exchange of the jet from the z to the x component in the jet-dominated regime, are significantly larger than those in the crossflow-dominated and transitional regimes. The axial and lateral normal turbulence intensities may even attain 85 and 150%, respectively, which are certainly beneficial to the mixing between the jet and the crossflow fluids. The axial and lateral normal turbulence intensities along the central streamline around the impact and bend over regions are larger than those in the jet-wake and the tube-wake regions. For instance, although not shown, $\sqrt{(\overline{u'^2})}/u_w$ is about 70% in the jet wake and 50% in the interface area and tube wake and $\sqrt{(\overline{w'^2})}/u_w$ is about 50% in the jet wake, 40% in the interface area, and 30% in the tube wake. Both the axial and the lateral normal turbulence intensities in the jet wake are higher than those in the tube wake, which is similar to the result obtained by Andreopoulos.[20] Nevertheless, the impact and the shear effects developed by the crossflow around the jet-turning area can induce larger turbulence strength than the wake region. In the far downstream area $x/d > 25$, the turbulence strengths in the transitional and the jet-dominated regimes get to almost the same levels: about 10% for $\sqrt{(\overline{u'^2})}/u_w$, 8% for $\sqrt{(\overline{w'^2})}/u_w$, and almost zero for the shear stress $\overline{u'w'}/u_w^2$. Impingement and shear developed by the crossflow and the bend over of the jet are apparently the most important mechanisms for turbulence generation in this type of flows.

Conclusions

The elevated jet in the crossflow presents complex near-wake flow patterns in different regimes of jet-to-crossflow momentum flux ratio. Three characteristic flow regimes, crossflow-dominated, transitional, and jet-dominated regimes, are identified. Drastic differences between the flow patterns existing in different regimes are induced by different extents of jet-shear and tube-tip downwash effects that influence the jet and the tube wakes at different jet-to-crossflow momentum flux ratios. In the crossflow-dominated regime, the downwash effect overwhelms the up-shear effect of the jet. A downwash area in the tube wake and a vortex in the jet wake are features of the flowfield. In the transitional regime, three types of complex flow patterns with jet-wake and tube-wake vortices are found. In the jet-dominated regime, no recirculation bubble is found in the jet wake or the tube wake due to a strong up-shear effect of the jet. The flow structures in the horizontal planes reveal that the recirculation bubbles in both the jet wake and the tube wake are unstable foci. Around the interface area, stable foci may be found. The geometry and turbulence properties of the jet central streamline reflect the impact effects of the crossflow on the jet. The turbulence properties along the central streamlines show that significant turbulences occur around the area of impingement, which is induced by the crossflow on the jet and the region of jet turning. The axial and transverse turbulence intensities, as well as the Reynolds shear stress around the impingement and the jet-turning regions, attain large values in the jet-dominated regime.

References

[1]Jordinson, R., "Flow in a Jet Directed Normal to the Wind," Aeronautical Research Council, R&M 3074, London, Oct. 1956.

[2]Keffer, J. F., and Baines, W. D., "The Round Turbulent Jet in a Cross-Wind," *Journal of Fluid Mechanics*, Vol. 15, No. 4, 1963, pp. 481–496.

[3]Margason, R. J., "The Path of a Jet Directed at Large Angles to a Subsonic Free Stream," NASA TN D-4919, 1968.

[4]Pratte, B. D., and Baines, W. D., "Profiles of the Round Turbulent Jet in a Cross Flow," *Journal of the Hydraulics Division, ASCE*, Vol. 93, No. HY6, 1967, pp. 53–64.

[5]Ramsey, J. W., and Goldstein, R. J., "Interaction of a Heated Jet with a Deflecting Stream," American Society of Mechanical Engineers, ASME Rept. 71-HT-2, 1971.

[6]Kamotani, Y., and Greber, I., "Experiments on a Turbulent Jet in a Cross-flow," *AIAA Journal*, Vol. 10, No. 11, 1972, pp. 1425–1429.

[7]Fearn, R., and Weston, R., "Vorticity Associated with a Jet in a Cross-flow," *AIAA Journal*, Vol. 12, No. 12, 1974, pp. 1666–1671.

[8]Rudinger, G., and Moon, L., "Laser-Doppler Measurements in a Subsonic Jet Injected into a Subsonic Cross Flow," *Journal of Fluids Engineering*, Vol. 98, Sept. 1976, pp. 516–520.

[9]Crabb, D., Durao, D. F. G., and Whitelaw, J. H., "A Round Jet Normal to a Crossflow," *Journal of Fluids Engineering*, Vol. 103, No. 1, 1981, pp. 142–153.

[10]Andreopoulos, J., and Rodi, W., "Experimental Investigation of Jets in a Crossflow," *Journal of Fluid Mechanics*, Vol. 138, 1984, pp. 93–127.

[11]Andreopoulos, J., "On the Structure of Jets in a Crossflow," *Journal of Fluid Mechanics*, Vol. 157, 1985, pp. 163–197.

[12]Sherif, S. A., and Pletcher, R. H., "Measurements of the Flow and Turbulence Characteristics of Round Jets in Crossflow," *Journal of Fluids Engineering*, Vol. 111, June 1989, pp. 165–171.

[13]Blanchard, J. N., Brunet, Y., and Merlen, A., "Influence of a Counter Rotating Vortex Pair on the Stability of a Jet in a Cross Flow: An Experimental Study by Flow Visualizations," *Experiments in Fluids*, Vol. 26, 1999, pp. 63–74.

[14]McMahon, H. M., Hester, D. D., and Palfrey, J. G., "Vortex Shedding from a Turbulent Jet in a Cross-Wind," *Journal of Fluid Mechanics*, Vol. 48, 1971, pp. 73–80.

[15]Kelso, R. M., Lim, T. T., and Perry, A. E., "An Experimental Study of Round Jets in Cross-Flow," *Journal of Fluid Mechanics*, Vol. 306, 1996, pp. 111–144.

[16]Morton, B. R., and Ibbetson, A., "Jets Deflected in a Crossflow," *Experiments in Thermal Fluid Science*, Vol. 12, No. 2, 1996, pp. 112–123.

[17]Fric, T. F., and Roshko, A., "Vortical Structure in the Wake of a Transverse Jet," *Journal of Fluid Mechanics*, Vol. 279, 1994, pp. 1–47.

[18]Brizzi, L. E., Foucault, E., and Bousgarbiès, J.-L., "Vortices Organization in the Near Field of a Jet Issuing Normally into a Crossflow," *Journal of Flow Visualization and Image Processing*, Vol. 5, No. 1, 1998, pp. 17–28.

[19]Moussa, Z. M., Trischka, J. W., and Eskinazi, S., "The Near Field in the Mixing of a Round Jet with a Cross-Flow," *Journal of Fluid Mechanics*, Vol. 80, Pt. 1, 1977, pp. 49–80.

[20]Andreopoulos, J., "Wind Tunnel Experiments on Cooling Tower Plumes, Part I: In Uniform Cross Flow," American Society of Mechanical Engineers, ASME Paper 86-WA/HT-31, 1986.

[21]Andreopoulos, J., "Wind Tunnel Experiments on Cooling Tower Plumes, Part I: In Non-Uniform Cross Flow of Boundary Layer Type," American Society of Mechanical Engineers, ASME Paper 86-WA/HT-32, 1986.

[22]Eiff, O. S., Kawall, J. G., and Keffer, J. F., "Lock-in of Vortices in the Wake of an Elevted Round Turbulent Jet in a Crossflow," *Experiments in Fluids*, Vol. 19, No. 3, 1995, pp. 203–213.

[23]Eiff, O. S., and Keffer, J. F., "On the Structures in the Near-Wake Region of an Elevated Turbulent Jet in a Crossflow," *Journal of Fluid Mechanics*, Vol. 333, 1997, pp. 161–195.

[24]Glass, M., and Kennedy, I. M., "An Improved Seeding Method for High Temperature Laser-Doppler Velocimetry," *Combustion and Flame*, Vol. 29, 1978, pp. 333–335.

[25]Mei, R., "Velocity Fidelity of Flow Tracer Particles," *Experiments in Fluid*, Vol. 22, No. 1, 1996, pp. 1–13.

[26]Steele, W. G., Taylor, R. P., Burrell, R. E., and Coleman, H. W., "Use of Previous Experience to Estimate Precision Uncertainty of Small Sample Experiments," *AIAA Journal*, Vol. 31, No. 10, 1993, pp. 1891–1896.

[27]Perry, A. E., and Fairlie, B. D., "Critical Points in Flow Patterns," *Advances in Geophysics*, Vol. 18, No. B, 1974, pp. 299–315.

[28]Chong, M. S., and Perry, A. E., "A General Classification of Three-Dimensional Flow Fields," *Physics of Fluids A*, Vol. 2, No. 5, 1990, pp. 765–777.

[29]Perry, A. E., and Steiner, T. R., "Large-Scale Vortex Structures in Turbulent Wakes Behind Bluff Bodies. Part 1. Vortex Formation," *Journal of Fluid Mechanics*, Vol. 174, Pt. 2, 1987, pp. 233–270.

[30]Hunt, J. C. R., Abell, C. J., Peterka, J. A., and Woo, H., "Kinematic Studies of the Flows around Free or Surface-Mounted Obstacles; Applying Topology to Flow Visualization," *Journal of Fluid Mechanics*, Vol. 86, Pt. 1, 1978, pp. 179–200.

[31]Sucec, J., and Bowley, W. W., "Prediction of the Trajectory of a Turbulent Jet Injected into a Crossflowing Stream," *Journal of Fluids Engineering*, Vol. 98, Dec. 1976, pp. 667–673.

[32]Adler, D., and Baron, A., "Prediction of a Three-Dimensional Circular Turbulent Jet in Crossflow," *AIAA Journal*, Vol. 17, No. 2, 1979, pp. 168–174.

I. Gokalp
Associate Editor